Inorganic Chemistry

Article

pubs.acs.org/IC

Systematic Evolution from Uranyl(VI) Phosphites to Uranium(IV) Phosphates

Eric M. Villa,[†] Connor J. Marr,[†] Laurent J. Jouffret,[†] Evgeny V. Alekseev,*[,†,‡] Wulf Depmeier,[§] and Thomas E. Albrecht-Schmitt*[,†]

[†]Department of Civil Engineering and Geological Sciences and Department of Chemistry and Biochemistry, University of Notre Dame, 156 Fitzpatrick Hall, Notre Dame, Indiana 46556, United States

[‡]Forschungszentrum Jülich GmbH, Institute for Energy and Climate Research (IEK-6), 52428, Jülich, Germany

[§]Institut für Geowissenschaften, Universität zu Kiel, Ludevig-Meyn Strasse 10, 24118 Kiel, Germany

Supporting Information

ABSTRACT: Six new uranium phosphites, phosphates, and mixed phosphate−phosphite compounds were hydrothermally synthesized, with an additional uranyl phosphite synthesized at room temperature. These compounds can contain U^{VI} or U^{IV}, and two are mixed-valent U^{VI}/U^{IV} compounds. There appears to be a strong correlation between the starting pH and reaction duration and the products that form. In general, phosphites are more likely to form at shorter reaction times, while phosphates form at extended reaction times. Additionally, reduction of uranium from U^{VI} to U^{IV} happens much more readily at lower pH and can be slowed with an increase in the initial pH of the reaction mixture. Here we explore the in situ hydrothermal redox reactions of uranyl nitrate with phosphorous acid and alkali-metal carbonates. The resulting products reveal the evolution of compounds formed as these hydrothermal redox reactions proceed forward with time.

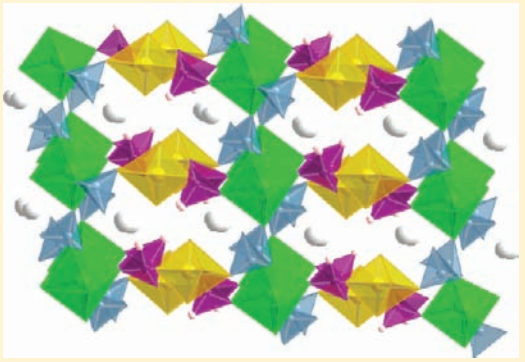

INTRODUCTION

The migration of actinides through the environment is of great concern and needs further investigation. The ability to confidently quantify the transport of actinides is important to our understanding of natural deposits but, more importantly, for the geological repositories where nuclear waste is, or could potentially be, stored. Uranium itself is not as great of a radiation hazard as many of the other actinides, but it does pose problems in terms of the vast quantities used in the nuclear industry. Phosphates are interesting in that they may help to mitigate transport owing to the generally low solubility of actinide phosphates. This has led to them being studied as possible long-term storage materials.[1−7]

Phosphite has many similarities to phosphate and phosphonate. However, a hydrogen atom has replaced one of the oxygen atoms in phosphate, and the phosphite anion contains no P−C bonds. However, phosphite can be used as a precursor for making phosphonates, and many actinide phosphonates have recently been synthesized.[8] In phosphite, the phosphorus atom is P^{III} instead of the normal P^{V}, as in phosphate, and this provides the opportunity for redox chemistry to take place. Unlike many other C_{3v} oxoanions, such as selenite, tellurite, or iodate,[9−11] there is now a hydrogen atom instead of the lone pair on the central atom of the anion; additionally, the phosphite anion is a strong reducing agent and should stabilize lower oxidation states for actinides. This reduction step is potentially useful because it could provide another way to limit the solubilities of the products formed owing to the generally lower solubility of U^{IV} versus U^{VI}.

Actinide phosphites are underexplored, but several compounds with atypical structures have been prepared through the application of organic templates.[12−18] Recently, we reported simple actinide(IV) phosphites that demonstrated the actinide contraction across the series and the influence of the starting oxidation state of the actinide used on the product composition.[19]

Uranium has two readily accessible oxidation states of 4+ and 6+, and while both states have extremely rich coordination chemistry, they also differ greatly in preferred coordination environments.[20] U^{IV} is commonly eight- or nine-coordinate, although its coordination numbers can vary from 6 to 12, and the distribution of ligands in its coordination sphere is largely isotropic. However, U^{VI} has two "yl" oxygen atoms, which give rise to the uranyl cation unit. Here the coordination environment is generally limited to tetragonal, pentagonal, or hexagonal bipyramids, and its geometries are highly anisotropic because of the short, terminal oxo atoms. These fundamental differences lead to divergent extended structures, with U^{IV} usually yielding 3D networks and U^{VI} being most often found

Received: January 12, 2012
Published: May 30, 2012

   dx.doi.org/10.1021/ic3000735 | *Inorg. Chem.* 2012, 51, 6548−6558

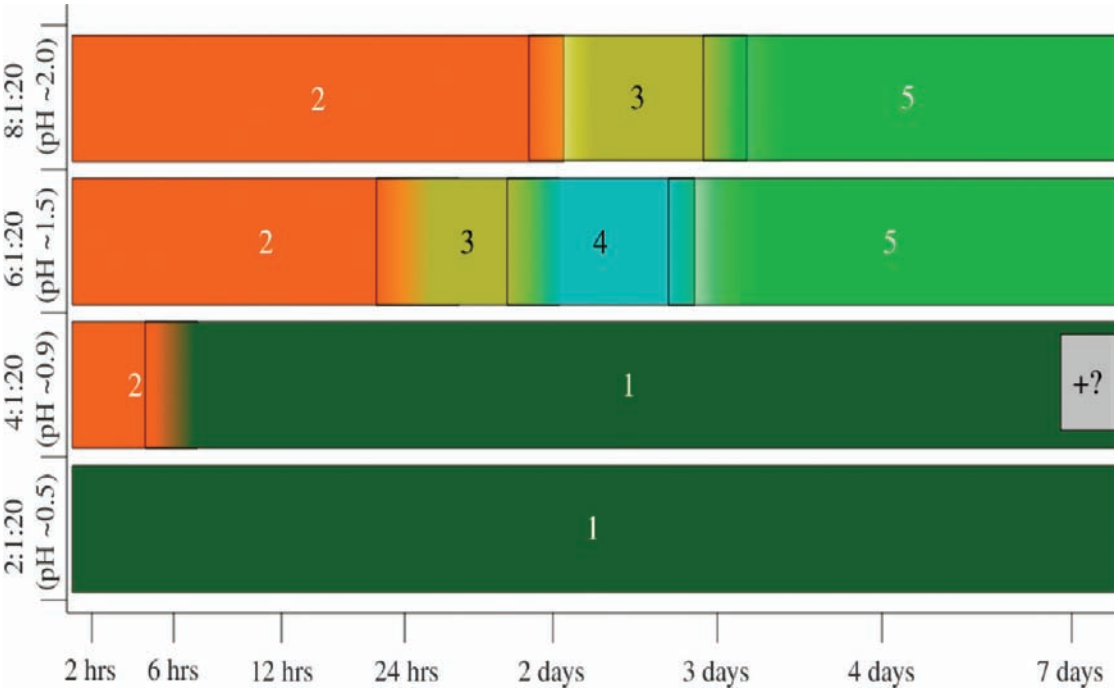

Figure 1. Cesium carbonate–uranyl nitrate–phosphorous acid system containing a ratio of 20:1 H_3PO_3–UO_2^{2+} as a function of the Cs_2CO_3 concentration and time. Ratios on the *y* axis are Cs_2CO_3–UO_2^{2+}–H_3PO_3. Here the products shown are **1**–**5**; all but **1** are new.[19] The overlapping colors and boxes indicate mixtures of compounds, and reactions were sampled at every point listed on the *x* axis.

in 2D sheets. Through the use of phosphite as a reducing ligand, there is also the possibility of making mixed-valent uranium compounds. While mixed-valent uranium materials are known, they are rare.[21,22]

Herein we will explore the alkali-metal carbonate–uranium phosphite system and attempt to understand the variables that determine product formation. The major influences on the products formed may be due to the phosphite concentration, starting pH, time, and alkali-metal cation used. We begin with a simple uranyl phosphite and expand to uranium(IV) phosphates. The seven compounds described herein illustrate the intrinsic complexity of the system and begin to illuminate their reaction pathways via room temperature and hydrothermal redox reactions.

EXPERIMENTAL SECTION

Caution! *While the $UO_2(NO_3)_2{\cdot}6H_2O$ used in this study contained depleted uranium, standard precautions for handling radioactive materials, such as uranyl nitrate, should be followed.*

Syntheses. Uranyl nitrate $UO_2(NO_3)_2{\cdot}6H_2O$ (International Bioanalytical Industries, Inc.), cesium carbonate (Alfa-Aesar, 99.9%), rubidium carbonate (Alfa-Aesar, 99%), and phosphorous acid (Alfa-Aesar, 97%) were used as received. All hydrothermal reactions were conducted in the same manner, unless otherwise listed. The reactants were mixed in their appropriate ratios and loaded into a 23 mL poly(tetrafluoroethylene) (PTFE) autoclave liner with 2 mL of distilled water. The liner was then sealed in a stainless steel autoclave and placed in a box furnace. The furnace was then ramped up to 200 °C for the desired number of hours (shown on the *x* axis of Figure 1) and then slowly cooled at a rate of 5 °C h^{-1}. Reactions were then washed with cold water, and the products were placed in a dish with ethanol for easier separation. The reaction conditions listed below represent the amounts and reaction times for the specific crystals obtained for single-crystal diffraction; however, these compounds can be made at all of the conditions shown in Figure 1, except the $Cs[UO_2(HPO_3)(H_2PO_3)]$ (**0**) structure, which was synthesized at room temperature conditions. Additionally, $U^{IV}(HPO_3)_2(H_2O)_2$ (**1**) was synthesized in our previous work and is shown in Figure 1 as it relates to the system.[19]

*$Cs[UO_2(HPO_3)(H_2PO_3)]$ (**0**).* Compound **0** was synthesized by dissolving 100.4 mg of uranyl nitrate (100 mM), 130.2 mg of Cs_2CO_3 (200 mM), and 327.4 mg of H_3PO_3 (1.996 M) in 2 mL of distilled water. The solution was then allowed to rest, undisturbed in a glass vial until crystallization occurred (~7 days). The approximate ratio of reactants is 2:1:20 Cs_2CO_3–U^{VI}–H_3PO_3. A few of the yellow-green blocks were suitable for crystallographic studies and yielded structure **0**, which crystallized in the space group $P\bar{1}$. The mother liquor was yellow and, when left to evaporate, yielded a viscous solution that only darkened in color. More crystals were not obtained from the solution, and it thus far the mother liquor has not dried completely, even while in an open vial.

*$Cs_2[(UO_2)_2(HPO_3)_3(H_2O)]$ (**2**).* This compound was synthesized by loading 101.2 mg of uranyl nitrate (101 mM), 391.1 mg of Cs_2CO_3 (600 mM), and 491.9 mg of H_3PO_3 (3.000 M) into a 23 mL PTFE autoclave liner with 2 mL of distilled water. This yields an approximate ratio of reactants of 6:1:30 Cs_2CO_3–U^{VI}–H_3PO_3. The liner was then sealed in a stainless steel autoclave, placed in a box furnace with the settings listed above, and heated at temperature for 2 h. Several of the yellow-orange columns were suitable for crystallographic studies and yielded structure **2**. Approximate yields for **2** range between 40 and 50%. Powder diffraction was also collected on the bulk crystals, and the predicted pattern correlates nicely with the collected data (see the Supporting Information).

*$Rb_2[(UO_2)_2(HPO_3)_3]$ (**2-Rb**).* The rubidium version of the previous compound (**2-Rb**) was synthesized by loading 99.9 mg of uranyl nitrate (99.5 mM), 370.5 mg of Rb_2CO_3 (802 mM), and 328.1 mg of H_3PO_3 (2.000 M) into a 23 mL PTFE autoclave liner with 2 mL of distilled water, which yields an approximate ratio of reactants of 8:1:20 Rb_2CO_3–U^{VI}–H_3PO_3. The liner was then sealed in a stainless steel autoclave, placed in a box furnace with the settings listed above, and heated at temperature for 2 h. Several of the light-yellow needles were suitable for crystallographic studies.

*$Cs_2[(UO_2)(U^{IV})(HPO_4)_2(HPO_3)_2]$ (**3**).* The first of the two mixed-valent uranium compounds was synthesized by loading 100.6 mg of uranyl nitrate (100 mM), 390.7 mg of Cs_2CO_3 (600 mM), and 328.0 mg of H_3PO_3 (2.000 M) into a 23 mL PTFE autoclave liner with 2 mL

dx.doi.org/10.1021/ic3000735 | *Inorg. Chem.* 2012, 51, 6548–6558

Table 1. Table of Crystallographic Data for All Listed Compounds: 0, 2, 2-Rb, 3, 3-Rb, 4, and 5[a]

	0	2	2-Rb	3	3-Rb	4	5
mol wt	1125.79	1061.81	950.93	1123.78	1316.94	1489.76	560.88
color and habit	yellow-green, block	yellow-orange, column	light yellow, needle	yellow-orange, block	orange-yellow, block	blue-green, block	green, plate
space group	$P\bar{1}$ (No. 2)	$P2_1/c$ (No. 14)	$P2_1/n$ (No. 14)	$P\bar{1}$ (No. 2)	$C2/c$ (No. 15)	$C2/m$ (No. 12)	$P2_1/m$ (No. 11)
a (Å)	7.9754(11)	10.7049(2)	11.1654(2)	6.8571(3)	16.2421(5)	25.7396(8)	7.7425(7)
b (Å)	10.5635(15)	11.8511(2)	11.3309(2)	11.1190(5)	10.5049(3)	5.5906(2)	5.6681(5)
c (Å)	10.6772(15)	12.6431(2)	12.1573(2)	12.0391(5)	11.0936(4)	7.6334(2)	9.1291(7)
α (deg)	94.147(3)	90	90	63.861(3)	90	90	90
β (deg)	95.880(3)	101.5850(10)	109.3760(10)	77.481(3)	98.7450(10)	98.964(2)	113.944(5)
γ (deg)	90.411(4)	90.00	90.00	79.331(3)	90.00	90.00	90.00
V (Å^3)	892.4(2)	1571.29(5)	1450.96(4)	800.22(6)	1870.80(10)	1085.03(6)	366.16(5)
Z	2	4	4	2	4	2	2
T (K)	103(2)	103(2)	100(2)	100(2)	100 (2)	100 (2)	100 (2)
ρ_{calcd} (g cm^{-3})	4.190	4.489	4.353	4.664	4.702	4.560	5.087
μ(Mo Kα) (cm^{-1})	225.74	255.20	293.47	251.73	315.07	261.69	275.07
R(F) for $F_o^2 > 2\sigma(F_o^2)$[b]	0.0312	0.0236	0.0451	0.0418	0.0271	0.0228	0.0188
$R_w(F_o^2)$[c]	0.0696	0.0523	0.0995	0.0971	0.0688	0.0519	0.0450

[a]The numbered compounds **2**–**5** relate to those found in Figure 1; compound **1** from Figure 1 is the previously published **1**, and [19] **2-Rb** and **3-Rb** are the rubidium versions of compounds **2** and **3**, respectively. [b]$R(F) = \sum||F_o| - |F_c||/\sum|F_o|$. [c]$R_w(F_o^2) = [\sum[w(F_o^2 - F_c^2)^2]/\sum wF_o^4]^{1/2}$.

of distilled water, which yields an approximate ratio of reactants of 6:1:20 Cs_2CO_3–U^{VI}–H_3PO_3. The liner was then sealed in a stainless steel autoclave, placed in a box furnace with the settings listed above, and heated at temperature for 24 h. Several of the yellow-orange blocks (**3**) were suitable for crystallographic studies.

*$Rb_2[(UO_2)_2(U^{IV})(PO_4)_2(HPO_3)_2(H_2O)]$ (**3-Rb**).* The second of the mixed-valent compounds was synthesized by loading 101.4 mg of uranyl nitrate (101 mM), 277.7 mg of Rb_2CO_3 (601 mM), and 328.5 mg of H_3PO_3 (2.003 M) into a 23 mL PTFE autoclave liner with 2 mL of distilled water. These amounts yield an approximate ratio of reactants of 6:1:20 Rb_2CO_3–U^{VI}–H_3PO_3. The liner was then sealed in a stainless steel autoclave, placed in a box furnace with the settings listed above, and heated at temperature for 24 h. Several suitable yellow-orange crystals (**3-Rb**) were obtained for crystallographic studies.

*$Cs_2[U^{IV}_3(PO_4)_2(HPO_3)_4]$ (**4**).* Compound **4** was synthesized by loading 101.1 mg of uranyl nitrate (100 mM), 391.8 mg of Cs_2CO_3 (601 mM), and 328.5 mg of H_3PO_3 (2.003 M) into a 23 mL PTFE autoclave liner with 2 mL of distilled water, which yields an approximate ratio of reactants of 6:1:20 Cs_2CO_3–U^{VI}–H_3PO_3. The liner was then sealed in a stainless steel autoclave, placed in a box furnace with the settings listed above, and heated at temperature for 48 h. Many of the blue-green blocks were suitable for crystallographic studies.

*$Cs[U^{IV}(PO_4)(HPO_4)_x(HPO_3)_{1-x}]$ (**5**), Where $x \leq 1$.* The listed compound was synthesized by loading 100.0 mg of uranyl nitrate (99.6 mM), 390.7 mg of Cs_2CO_3 (599 mM), and 327.2 mg of H_3PO_3 (1.995 M) into a 23 mL PTFE autoclave liner with 2 mL of distilled water. This yields an approximate ratio of reactants of 6:1:20 Cs_2CO_3–U^{VI}–H_3PO_3. The liner was then sealed in a stainless steel autoclave, placed in a box furnace with the settings listed above, and heated at temperature for 168 h. Many of the green plates were suitable for crystallographic studies. Approximate yields for **5** range between 70 and 75%. Powder diffraction was also collected on the bulk crystals, and the predicted pattern correlates nicely with the collected data (see the Supporting Information).

Crystallographic Studies. Crystals of all compounds were mounted on CryoLoops with Krytox oil and optically aligned on a Bruker APEXII Quazar X-ray diffractometer using a digital camera. Initial intensity measurements were performed using a IμS X-ray source and a 30 W microfocused sealed tube (Mo Kα, λ = 0.71073 Å) with high-brilliance and high-performance focusing Quazar multilayer optics. Standard *APEXII* software was used for determination of the unit cells and data collection control. The intensities of the reflections of a sphere were collected by the combination of an appropriate number of exposures (frames). Each set had a different φ angle for the crystal, and each exposure covered a range of 0.5° in ω. *SAINT* software was used for data integration including Lorentz and polarization corrections. Semiempirical absorption corrections were applied using the program *SCALE* (*SADABS*).[23] Crystallographic information for all obtained phases is summarized in Table 1. Atomic coordinates and additional structural information are provided in the Supporting Information (CIFs).

Powder diffraction was collected on a Bruker D8 Advance with DaVinci (Cu Kα, λ = 1.5405 Å) using a $\theta/2\theta$ geometry. The rotating sample was scanned from 2θ = 5° to 85° or 90° at a 0.02 increment and 15 s step^{-1}. Powder patterns were compared to calculated versions and can be found in the Supporting Information.

UV–vis–Near-IR (NIR) Spectroscopy. UV–vis–NIR data were acquired from single crystals using a CRAIC Technologies microspectrophotometer. Crystals were placed on quartz slides under Krytox oil, and the data were collected from 200 to 1600 nm. The exposure time was autooptimized by the CRAIC software. The characteristic peaks for U^{6+} and U^{4+} are listed with the acquired spectra (see the Supporting Information).

Raman Spectroscopy. Raman spectra were collected for crystals of **1**, **2**, and **5** to assist in determining the presence of the disordered phosphite in **5** (see the Supporting Information). The system used is a Bruker Sentinel system linked via fiber optics to a video-assisted Raman probe in a microscope mount. The laser wavelength is 785 nm with a power of 200 mW. The instrument is equipped with a high-sensitivity, TE-cooled 1024 × 255 CCD array. The spectra were collected in the range from 80 to 3200 cm^{-1}.

RESULTS AND DISCUSSION

The evolution of products in the cesium–uranium phosphite system is shown in Figure 1. It illustrates how changing the cesium carbonate concentration and reaction duration affects the products that form in these hydrothermal reactions. The lower the cesium carbonate concentration, the more likely the product is reduced to U^{IV} quickly. As the pH of the starting reaction solution is increased, we observe a slowing of the in situ reduction of uranium. Additionally, the products continue to evolve with time as the redox reactions continue to progress forward to U^{IV} compounds. Two rubidium–uranium phosphite

dx.doi.org/10.1021/ic3000735 | Inorg. Chem. 2012, 51, 6548–6558

or mixed phosphate−phosphite compounds were also synthesized and are described in the text after the appropriately related cesium phases.

Before exploring the hydrothermal reaction products listed above, we were able to isolate a simple uranyl phosphite at room temperature. Crystals of **0** were obtained via room temperature reaction of uranyl nitrate with cesium carbonate and phosphorous acid, with the ratio of 2:1:20 Cs_2CO_3−$UO_2(NO_3)_2{\cdot}6H_2O$−H_3PO_3. These crystals have $P\bar{1}$ symmetry and form pale-yellow-green blocks within a few days of mixing. The simple sheet-type structure is shown in Figure 2, top. The extended sheet contains two different phosphite ligands, one with a protonated oxygen atom and one without. Here all of the uranyl units are pentagonal bipyramids and have corner-sharing phosphite ligands, as shown in Figure 2, bottom.

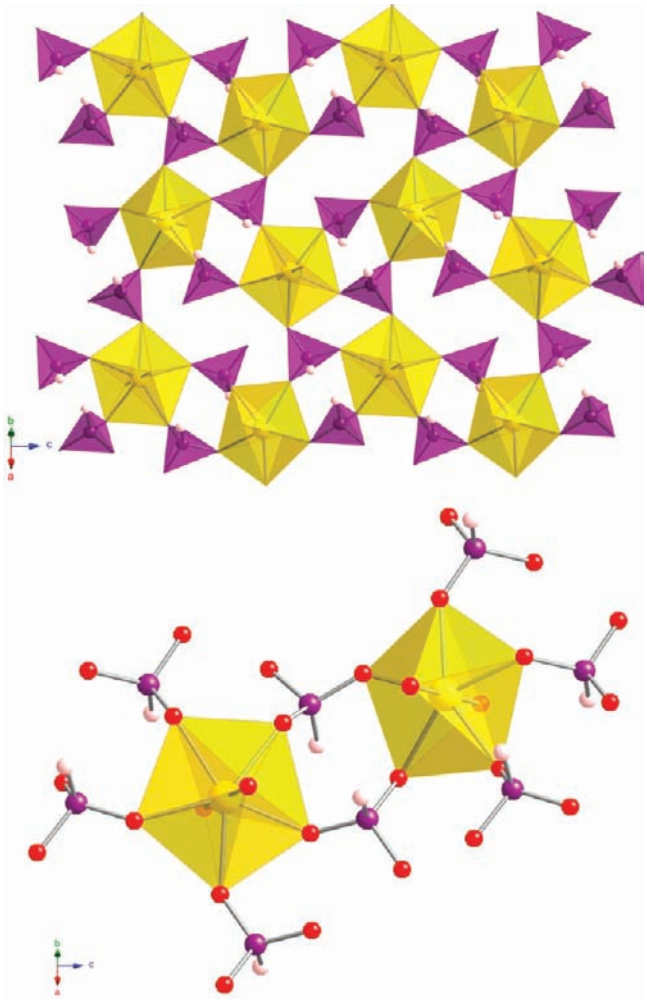

Figure 2. Top: Sheet of **0**, which crystallizes in the space group $P\bar{1}$, shown here with two types of phosphite ligands: one where all three oxygen atoms are bridging and one where only two are bridging, with the other being a terminal oxygen atom. Bottom: Local environments of uranyl pentagonal bipyramids and the corner-sharing phosphite ligands. In both parts, the uranyl units are yellow, the phosphorus atoms are purple, the oxygen atoms are red (omitted in the top for clarity), and the hydrogen atoms are white.

The average bond length for the U═O bonds of the uranyl unit is 1.788(4) Å, and the average U−O bond length for the five oxygen atoms in the equatorial plane of the pentagonal bipyramids is 2.376(4) Å. Again, there are two types of phosphite ligands: one that contains all μ_2-bridging oxygen atoms and one that contains two μ_2-bridging oxygen atoms and one terminal oxygen atom. The average bond length for these μ_2-oxo atoms is 1.516(5) Å. There is some shortening of the bond distances for the μ_2-oxygen atoms attached to the phosphite anions with terminal oxygen atoms. There is also considerable lengthening in the P−O distances in these protonated terminal oxo groups, which have an average bond of 1.578(5) Å [see the Supporting Information for bond valence sum (BVS) calculations]. The BVS values for the two uranium centers here are 5.972 and 6.024 Å.

If the ratio of Cs_2CO_3−$UO_2(NO_3)_2{\cdot}6H_2O$−H_3PO_3 is not within the correct window, phosphorous acid will reduce U^{VI} to U^{IV} even at room temperature. This shows the ability of phosphite to produce U^{IV} compounds readily if an excess is provided to interact with the uranium. However, the sheet topology in **0** is not the first of its type. In 1985, Mistryukov and Mikhailov published two other phosphites similar to this one but used rubidium and potassium instead of cesium to create $Rb[(UO_2(HPO_3)(H_2PO_3)](H_2O)_3$ and $K_2[UO_2(HPO_3)_2](H_2O)_2$, respectively.[15] The former is the same topology as that of **0**, but the latter potassium compound is quite different (as is indicated in the formula). In all three cases, the alkali-metal cations are acting as a charge balance between the uranyl phosphite sheets. This sheet type has also been seen in several different uranyl chromates, selenates, and molybdates, which was found by comparing the graphical topology representations proposed by Krivovichev and Burns.[24,25] These room temperature reactions proceed forward quickly, within 1 or 2 days, even in the absence of evaporation of the mother liquor.

In contrast, hydrothermal reactions of uranium with phosphorous acid yield a rich system where small changes in the reaction conditions give very different products (all hydrothermal reactions were conducted at 200 °C unless otherwise stated). Furthermore, only **2** and **5** could be made as pure phases; compounds **2-Rb**, **3**, **3-Rb**, and **4** were individually picked from their reaction product mixtures for single-crystal X-ray diffraction. As stated in our previous work, if the pH of the starting solution is kept lower (i.e., using less cesium carbonate), a dense 3D network of uranium(IV) phosphite is produced.[19] **1** is easily formed at these low pH values and is quite stable with time. While the yield is always low for these reactions, the only crystals found were the uranium(IV) phosphite listed above. The mother liquor from these reactions is dark green and persists even when exposed to air over a long period of time. Thus far, no crystals have precipitated out of these solutions, and only a dark-green, viscous solution is yielded owing to the apparent high solubility of uranium(IV) phosphite.

The most readily formed hydrothermal reaction product in this system with U^{VI} is **2**. In general, this product is easily formed at short reaction times and with a significant amount of Cs_2CO_3 to increase the pH of the starting reaction mixture. Crystals of this simple uranium(VI) phosphite are yellow-orange needles and crystallize in the monoclinic space group $P2_1/c$. As one increases the phosphite concentration, the crystals of this product also increase in size. A general ratio of reactants for this product is 8:1:20 Cs_2CO_3−$UO_2(NO_3)_2{\cdot}6H_2O$−H_3PO_3. In contrast to the room temperature uranium(VI) phosphite (**0**), in **2**, there is only one type of phosphite ligand, which contains all μ_2-bridging oxygen atoms (the sheet is shown in Figure 3, top).

dx.doi.org/10.1021/ic3000735 | Inorg. Chem. 2012, 51, 6548−6558

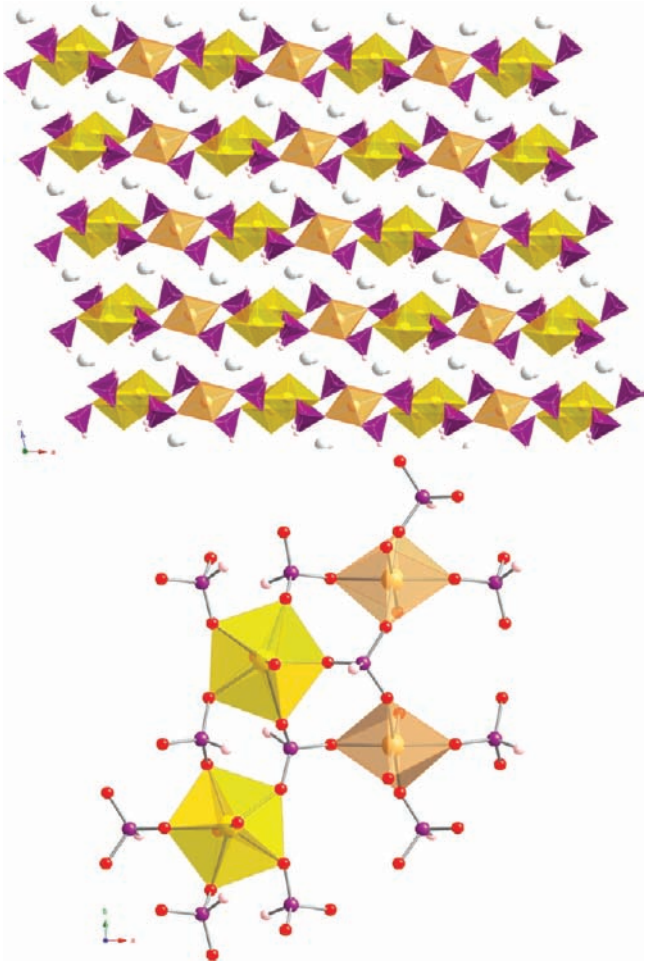

Figure 3. Top: 2D sheet of **2** as viewed in the *ac* plane. The cesium balances charge between the sheets. This hydrothermally synthesized cesium uranyl phosphite crystallizes in the space group $P2_1/c$. Bottom: Two different uranyl sites. The yellow polyhedra represent the uranyl pentagonal bipyramids, whereas the light-orange polyhedra represent the uranyl square bipyramids. In both the top and bottom, the phosphorus atoms are purple, the oxygen atoms are red (omitted in the top for clarity), and the hydrogen atoms are white.

The 2D sheet of **2** is different from the room temperature version (**0**) because there are no η-oxygen atoms attached to the phosphite ligands. We now also have two different uranyl units: one is a pentagonal bipyramid, shown in yellow, and the other is a square bipyramid, shown in light orange (Figure 3, bottom). However, like the room temperature uranyl phosphite (**0**), all of the phosphites here are corner-sharing with the uranyl units. The average bond lengths for the uranyl oxygen atoms are 1.786(4) and 1.784(5) Å for the pentagonal and square bipyramids, respectively. The U−O bond lengths in the equatorial plane for the pentagonal bipyramids are an average of 2.363(4) Å. Conversely, the U−O bonds for the square bipyramids are shorter at 2.280(5) Å. The calculated BVS values for the two uranyl units here are 6.075 Å for the pentagonal bipyramids and 5.922 Å for the square bipyramids. Here, all of the phosphite ligands contain μ_2-oxo groups and have an average bond length of 1.522(5) Å.

Additionally, we can make the rubidium version of this compound, **2-Rb**. The main differences between these two structures are the absence of the cocrystallized water molecules in the rubidium structure and the orientation of the phosphite ligands (Figure 4). The layers are now packed in different ways; two rubidium cations now reside in a gap that was previously

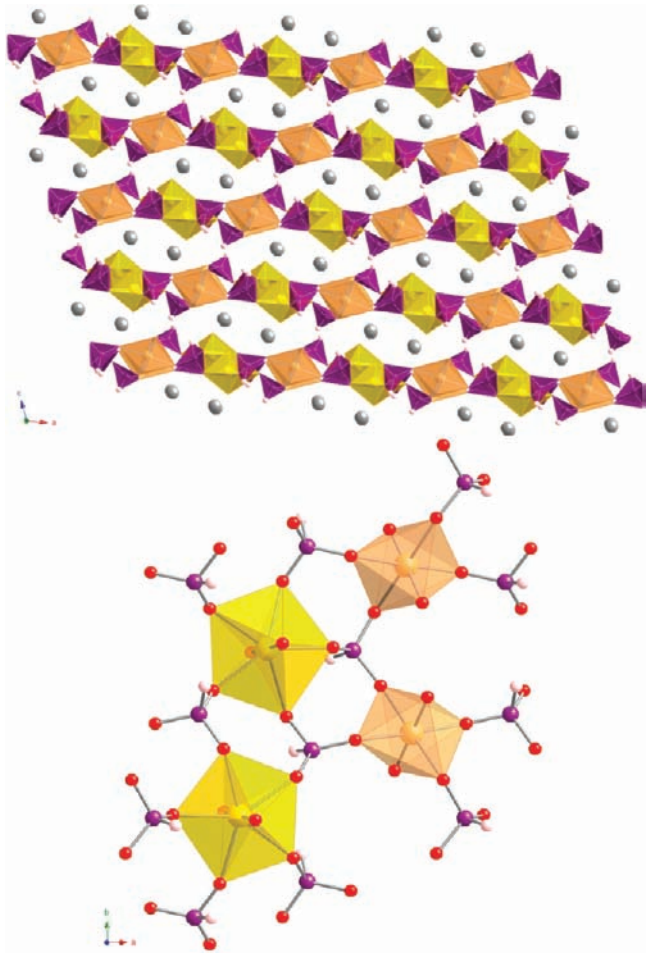

Figure 4. Top: 2D sheet of **2-Rb**, which crystallizes in the space group $P2_1/n$, as viewed down the *b* axis with the rubidium cations in the interlayers (shown in gray). The sheets and orientation of the phosphite ligands are changed by the presence of this smaller cation. Bottom: Two uranyl sites, with the yellow and light-orange polyhedra representing the uranyl pentagonal and square bipyramids, respectively. In both the top and bottom, the phosphorus atoms are purple, the oxygen atoms are red (omitted in the top for clarity), and the hydrogen atoms are white.

only occupied by one cesium ion. Either because of this change or as a result thereof, the phosphites have changed their arrangement. In the cesium version (**2**; Figure 3), when looking at the sheet in the *ac* plane and using the hydrogen atoms for reference, the phosphite ligands between the two types of uranyl units are pointing away from each other. Conversely, in the rubidium structure, these same phosphites are pointing in the same direction. In general, however, the two structures are still quite similar and contain the same building blocks, pentagonal and square bipyramids. Here the average bond lengths for the uranyl oxygen atoms are 1.756(12) and 1.789(8) Å for the pentagonal and square bipyramids, respectively. The bond lengths for the equatorial oxygen atoms are 2.382(9) Å for the pentagonal bipyramids and 2.286(7) Å for the square bipyramids, showing some lengthening in the equatorial plane in comparison to the cesium version. Additionally, the BVS values for the U^{VI} units in

dx.doi.org/10.1021/ic3000735 | *Inorg. Chem.* 2012, 51, 6548−6558

this structure are 5.863 Å (square bipyramids) and 6.178 Å (pentagonal bipyramids). Unlike the U−O bond distances, the P−O distances in the phosphite ligands are very similar to the previous cesium type at 1.521(8) Å. Both **2** and **2-Rb** share a known typology that has been seen in both neptunyl chromates and uranyl selenates.[25,26] The referenced compounds are sheets of uranyl (or neptunyl) pentagonal bipyramids made up of two types of uranyl chains: one pentagonal bipyramid linked by five corner-sharing ligands, which are then cross-linked by another chain of pentagonal bipyramids linked by only four corner-sharing ligands (leaving one terminal oxo unit on the uranyl unit). However, in both **2** and **2-Rb**, we again have two types of uranyl chains linked into sheets, but here there are pentagonal bipyramids with five corner-sharing ligands, which are now cross-linked by square bipyramids with four corner-sharing ligands. Although compounds **2** and **2-Rb** and the referenced compounds above contain different actinyl coordination environments, the graphical topology representations they create are identical.

Looking back at Figure 1, as we heat the reactions with higher cesium carbonate concentrations, new products begin to form. When heating 6:1:20 for 24 h, a new and very interesting product forms. Here we slowly oxidize the phosphite and, likewise, reduce U^{VI} to finally be able to isolate a mixed U^{VI}/U^{IV}, mixed phosphate−phosphite compound. Figure 5 shows the extended structure of **3**. In our first example of a mixed $U^{VI/IV}$ and $P^{III/V}$ structure, the closely packed 3D network is made up of layers of uranium(VI) phosphite and uranium(IV) phosphate. The yellow-orange block crystals were suitable for single crystallographic studies and were found to have $P\bar{1}$ symmetry. Here there are two different uranium sites, the first of which is the pentagonal bipyramid of U^{VI}. This site is coordinated by four corner-sharing phosphites and one corner-sharing phosphate ligand, where the average uranyl U═O bond length is 1.782(8) Å and the average U−O bond length for the equatorial oxygen atoms is 2.363(8) Å. The other site contains a U^{IV} atom that is seven-coordinate; five of these are corner-sharing phosphates, and the other two are corner-sharing phosphites; here the average U−O bond length is 2.301(8) Å. Here the BVS value for U^{VI} is 6.142 Å, and it is 4.215 Å for U^{IV}. The phosphite P−O bond lengths here are an average of 1.516(7) Å, the μ_2-bridging oxygen atoms in the phosphate ligands average 1.518(6) Å, and the terminal protonated P−O distances in phosphates average 1.612(9) Å (see the Supporting Information for BVS calculations).

This mixed-valent compound is compact and leaves little room for the cesium cations that are in the 3D network. This compound is important because it serves as a window into the redox chemistry that is occurring in these hydrothermal reactions. In structure **3**, half of the uranium atoms are U^{VI} and half are U^{IV}. Likewise, half of the phosphorus atoms in the structure are P^{V} and the other half are P^{III}. At these higher pH conditions, reduction of uranium is much slower than it was at the lower pH values. The pH values of the starting reaction solutions are able to inhibit this redox chemistry so that a more stepwise progression of the products can be followed. Now that an appropriate window is available, products can be monitored as the oxidation−reduction chemistry of this system progresses.

In addition to the compound described above, the rubidium salt of the mixed $U^{VI/IV}$ was also synthesized, **3-Rb**. The reactant ratios were a bit more flexible for the formation of this product. Here, time was the most important in its formation. The mixed rubidium−uranium, mixed phosphate−phosphite

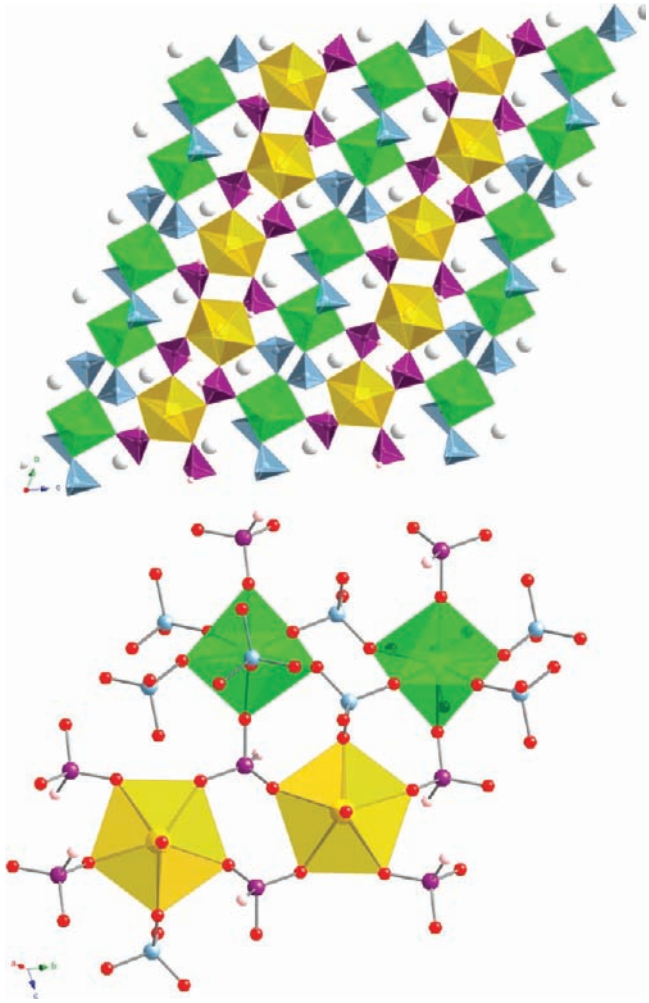

Figure 5. Top: Dense 3D network of **3** viewed in the *bc* plane and having $P\bar{1}$ symmetry. Bottom: Two different uranium centers, one a pentagonal bipyramid of U^{VI} and one a seven-coordinate U^{IV}. The structure can be viewed as alternating layers of uranyl(VI) phosphite and uranium(IV) phosphate. The U^{VI} polyhedra are in yellow, the U^{IV} polyhedra are in green, phosphates are in light blue, phosphites are in purple, the cesium cations are in light gray (top only), and the oxygen atoms are shown in red (bottom only).

structures are very different from the cesium structure. Instead of the uranium sites containing only corner-sharing ligands, here U^{VI} form edge-sharing dimers (Figure 6). This addition completely alters the overall structure for this extended solid. The structure consists of U^{VI} dimers linked to other dimers via a corner-sharing phosphite ligand. This forms a U^{VI} layer, which is then connected to other U^{VI} layers by a U^{IV} monomer. The rubidium atoms then help to balance the charge by sitting in the small openings in this 3D network.

As shown in Figure 6 (bottom), the two U^{VI} pentagonal bipyramids are edge-sharing and are each coordinated by two phosphates and two phosphites. Here the average uranyl U═O bond length is 1.779(5) Å. In the equatorial plane, the average U−O bond length is 2.371(5) Å. While both of the phosphites are corner-sharing, one of the phosphates is edge-sharing and the other one is corner-sharing. It is at these edge-sharing phosphates that the two uranyl pentagonal bipyramids are linked together. Additionally, this edge-sharing phosphate along with a corner-sharing phosphite link the U^{VI} dimer to the U^{IV} unit. The U^{IV} units in the structure link the layers of U^{VI} dimers

dx.doi.org/10.1021/ic3000735 | Inorg. Chem. 2012, 51, 6548−6558

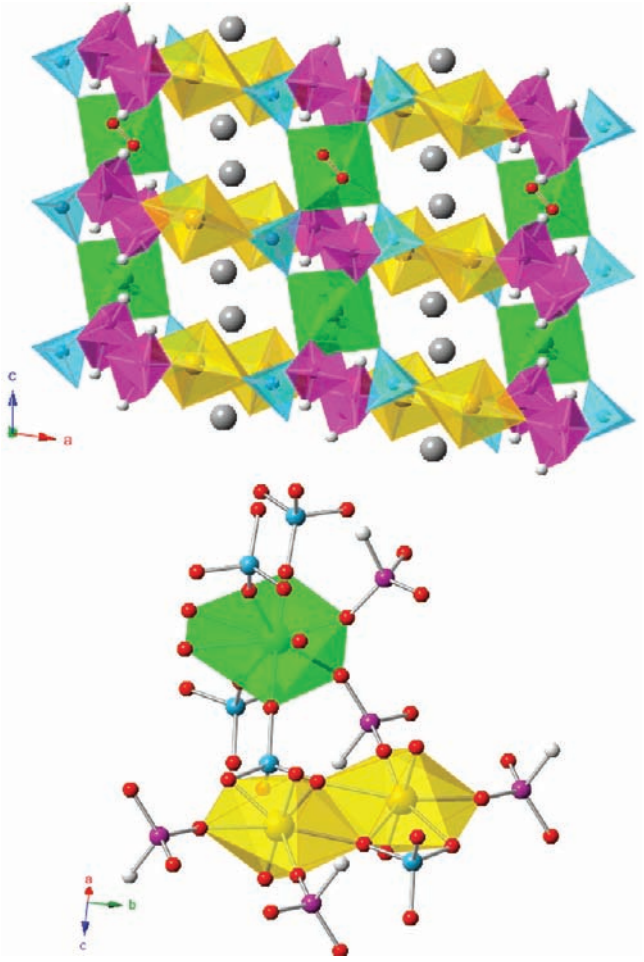

Figure 6. Top: More-open, mixed-oxidation-state 3D network of **3-Rb** shown in the *ac* plane and crystallizing in the space group *C*2/*c*. The layers of U^{VI} dimers are linked together by U^{IV} polyhedra. Bottom: Seven-coordinate U^{IV} and the dimer of pentagonal bipyramids of U^{VI}. The U^{VI} polyhedra are in yellow, the U^{IV} polyhedra are in green, phosphates are in light blue, phosphites are in purple, the rubidium atoms are in dark gray (top only), and the oxygen atoms are in red (bottom only).

together. The BVS values here are quite similar to those of the previous cesium structure with that for U^{VI} at 6.099 Å and that for U^{IV} at 4.208 Å. In **3-Rb**, the average bond lengths for the phosphate P−O distances are 1.530(5) Å and the average P−O phosphite distances are 1.494(7) Å.

The U^{IV} atom is seven-coordinate and has four phosphates, two phosphites, and a terminal water. The bridging oxygen atoms are an average of 2.376(5) Å, whereas the terminal water is considerably longer at 2.498(10) Å. In this diagram, the terminal oxygen atom looks to be two oxygen atoms, but this is due to symmetry disordering. All of the phosphates and phosphites are corner-sharing on this U^{IV} atom. Together these two uranium building blocks help to build the more open of the two mixed uranium and mixed phosphate−phosphite 3D networks. Additionally, the symmetry of this structure is higher at *C*2/*c* instead of $P\bar{1}$ from the cesium version. While many attempts have been made to make these compounds with the other alkali metals, they have thus far been unsuccessful.

If the reaction conditions are kept the same as those for the cesium mixed $U^{VI/IV}$ product but the reaction time is extended out further, we see complete reduction of the uranium to U^{IV} within the structure. Here we find a U^{IV} structure that contains both phosphate and phosphite ligands. The 3D network of the extended structure **4** has channels running down the *b* axis (Figure 7, top) and has *C*2/*m* symmetry. Chemically, this

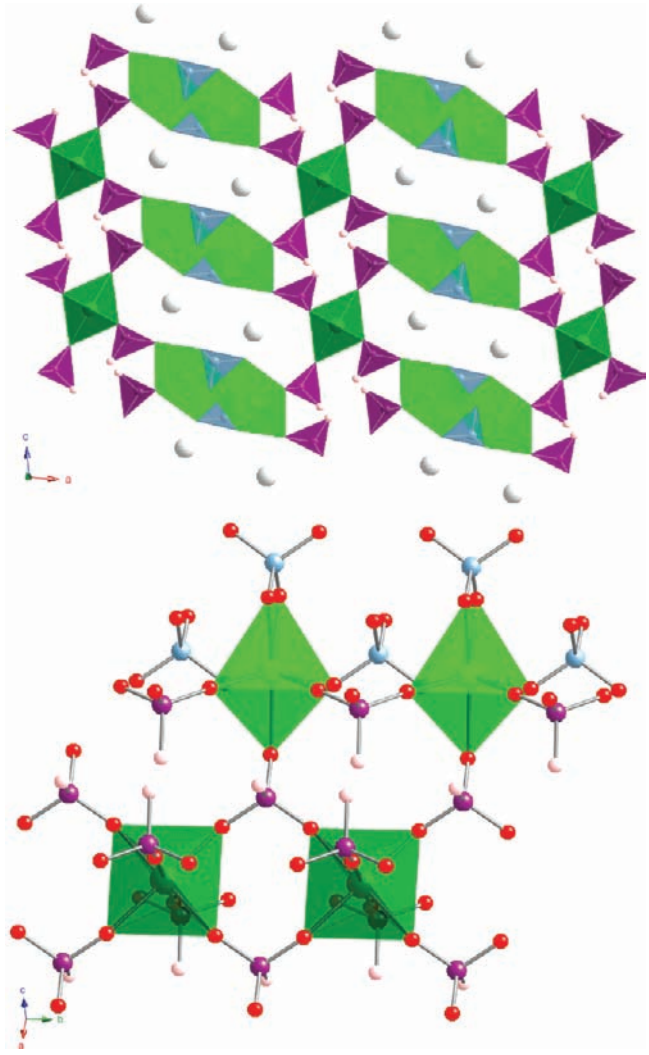

Figure 7. Top: 3D network of **4** in the *ac* plane and having *C*2/*m* symmetry. Two different U^{IV} polyhedra with both phosphate and phosphite yield this channel type structure. Bottom: Two different U^{IV} sites, with the seven-coordinate site in light green and the six-coordinate site in dark green. The former has three corner-sharing phosphites, two corner-sharing phosphates, and one edge-sharing phosphate, whereas the latter has six corner-sharing phosphites. Here the U^{IV} polyhedra are in light and dark green, phosphates are in light blue, phosphites are in purple, the cesium atoms are light gray (top only), and the oxygen atoms are in red (bottom only).

compound is a logical progression from the previous cesium structure, where there was both U^{VI} and U^{IV}, and now we have completely reduced all of the uranium to U^{IV}.

When looking at the overall structure for **4** in Figure 7, one can see the open nature for this U^{IV} structure. There are two types of U^{IV} atoms here, one that is seven-coordinate and one that is six-coordinate, with average bond lengths of 2.331(4) Å for the former and 2.228(4) Å for the latter. Here the two U^{IV} centers give BVS values at 3.947 and 4.388 Å, respectively. The value is a bit high for the six-coordinate U^{IV} but is quite good for the seven-coordinate U^{IV}. The P−O phosphite bond lengths

dx.doi.org/10.1021/ic3000735 | *Inorg. Chem.* 2012, 51, 6548−6558

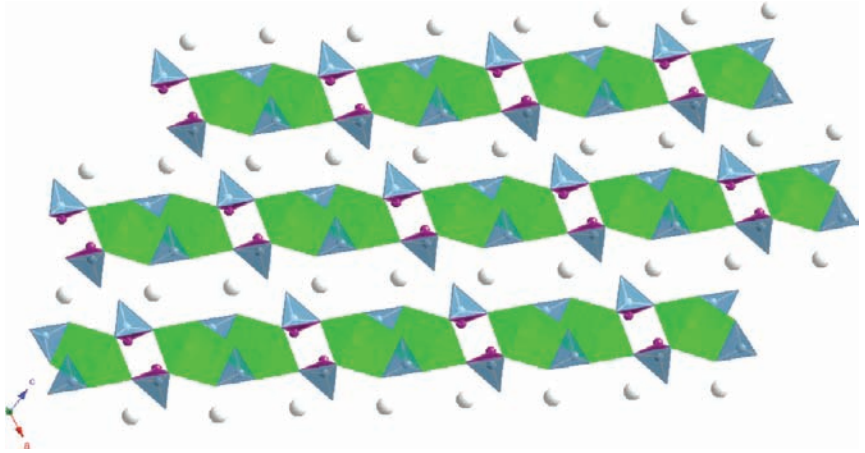

Figure 8. 2D sheet of **5**, as viewed in the *ac* plane. The phosphate−phosphite disordering can be seen between the linked chains and has $P2_1/m$ symmetry. Here the U^{IV} polyhedra are in light green, the phosphate polyhedra are in light blue, the phosphite polyhedra are in purple, and the cesium atoms are in light gray.

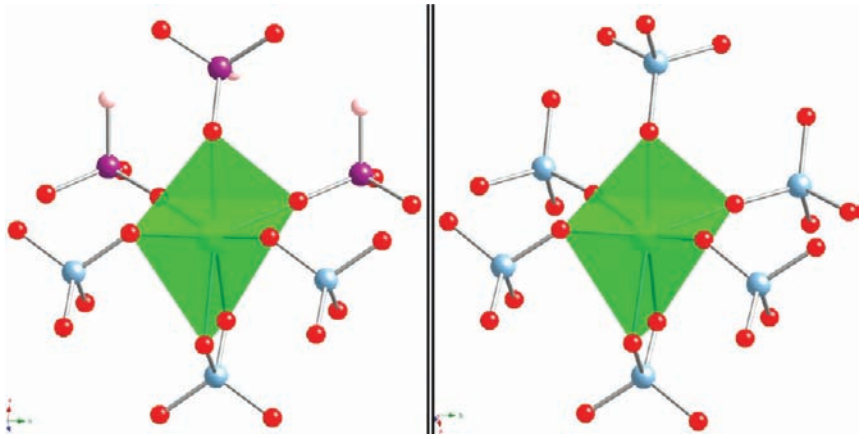

Figure 9. Comparison of the two seven-coordinate U^{IV} sites in **4** and **5**, with the former on the left and the latter on the right. The two are almost identical in bonding environments around the uranium (phosphite disordering has been removed from the right for clarity). Here the U^{IV} polyhedra are in light green, phosphates are in light blue, phosphites are in purple (left only), and the oxygen atoms are in red.

average at 1.515(4) Å and the phosphate P−O distances average at 1.534(5) Å. With only three oxygen atoms for bridging and a hydrogen atom on the phosphorus, the phosphite ligands appear to be directing this 3D structure. The cesium atoms are in the channels, which run down the *b* axis, and act as charge balances.

The two U^{IV} sites in this extended structure have very different coordination environments. The seven-coordinate U^{IV}, shown in light green in Figure 7 (bottom), has three corner-sharing phosphites, two corner-sharing phosphates, and one edge-sharing phosphate. It is these phosphates that link the seven-coordinate U^{IV} atoms together throughout the structure. Each phosphate in the structure is edge-sharing with one of the seven-coordinate U^{IV} atoms and corner-sharing with two others. Capping the chain of alternating U^{IV} and phosphates are phosphite ligands.

The six-coordinate U^{IV}, shown in dark green, in this structure is almost perfectly octahedral in geometry, with the two axial ligands slightly shorter than the four in the equatorial plane. The four equatorial phosphites are corner-sharing between two six-coordinate U^{IV} atoms and one seven-coordinate U^{IV} atom, whereas the two axial phosphites are corner-sharing with one six-coordinate and two seven-coordinate U^{IV} atoms. This U^{IV} mixed phosphate−phosphite structure is a clear progression from the mixed U^{VI}−U^{IV} mixed phosphate−phosphite structure discussed above. As the series has developed, more and more reduction of the uranium has occurred until we now have a completely reduced U^{IV} structure. Again, while attempts have been made with other alkali metals to obtain a similar structure, they have thus far been unsuccessful.

The last compound in the series virtually completes this evolution of products with time. Again, when the reaction conditions are kept the same as above but the length of the reaction is extended further to 96 h and beyond, a new U^{IV} product forms that contains almost exclusively phosphate ligands. Here we have completely reduced the uranium in the structure to U^{IV} and almost completely oxidized all of the phosphite to phosphate. The product **5** crystallizes in the space group $P2_1/m$ and is shown in Figure 8. Crystallographically, it appears that the mixed phosphate−phosphite site in the structure is approximately 80% phosphate and 20% phosphite (see the Supporting Information for Raman spectra).

The layered structure of **5** is shown in Figure 8, where the mixed phosphate−phosphite site can clearly be seen within the sheet structure. While the cesium atom is between the sheets themselves, this uranium topology is extremely similar to that of the previous 3D U^{IV} mixed phosphate−phosphite structure. In fact, this structure also contains a seven-coordinate U^{IV} atom,

dx.doi.org/10.1021/ic3000735 | *Inorg. Chem.* 2012, 51, 6548−6558

which has almost the exact same geometry as that of the previous seven-coordinate U^{IV} site. Here the average bond U−O bond length is 2.330(3) Å, which is only slightly shorter than the average bond lengths in the seven-coordinate U^{IV} in **4**. Here the one U^{IV} center has a BVS value of 3.956 Å. In **5**, the phosphate P−O bond lengths average 1.530(4) Å and the disordered phosphite P−O bond lengths are an average of 1.483(9) Å. There is also one protonated, terminal oxygen atom on the HPO_4^{2-} unit (see the Supporting Information for BVS calculations). In Figure 9, the two geometries are compared, with the phosphate−phosphite disordering removed for clarity (however, it is the top three phosphates in the structure on the right where phosphite disordering occurs).

On the left is the seven-coordinate **4**, and on the right is the seven-coordinate U^{IV} site from **5**. Both contain five corner-sharing ligands and one edge-sharing phosphate ligand, and the overall environments are virtually identical, with the average bond lengths being very similar. More importantly is how the phosphite helps to direct the structure into a 3D network. Without any phosphite, or at least in a very limited quantity, the uranium will take on a sheet-type structure after it has all been reduced from U^{VI} to U^{IV} and all of the P^{III} has been oxidized to P^{V}. After this mixture is reacted for over 7 days, this seems to be the final phase formed; however, it may be safe to assume that the next structure may be the same topology as that of **5**, just without phosphite disordering.

Along with the products being isolated as described in the Experimental Section, some of the products could be synthesized in another way. For example, the mixed-valent cesium−uranium compound **3** was synthesized initially by heating the starting materials for 24 h and then cooling, but it can also be made by starting with **2** as the uranium source. **2** was obtained after only 2 h at 200 °C, so to create compound **3** again, the reaction conditions were not changed from the initial synthesis. A relative ratio of 6:1:20 Cs_2CO_3−U^{VI}−H_3PO_3 was used with the new source of uranium; the reaction was heated to 200 °C for 24 h and then cooled. The only product obtained was that of **3**.

The evolution of products throughout this cesium−uranium phosphite series has led to some interesting conclusions on what is causing these different species to form. The clearest one is time. As the reactions are allowed to react, we see a continual reduction of U^{VI} to U^{IV} and, in most cases, have a final product consisting of almost exclusively uranium(IV) phosphate. The second significant influence on these reaction products is the amount of cesium carbonate used. As higher concentrations are used, we see a slowing of the redox chemistry and are able to reveal more compounds that are of mixed-valency, for both uranium and phosphorus. This could be due to one of three things: the pH, cation concentration, or ionic strength.

To investigate this more thoroughly, reactions were conducted at low pH and high phosphite concentration, where only one product was formed, uranium(IV) phosphite (**1**). Under these conditions, we are reducing all of U^{VI} to U^{IV} and still have an excess of phosphorous acid to incorporate only phosphite into the structure. Several different cesium salts were then employed in an effort to raise the cation concentration and also the ionic strength to see if these were the reasons for the slowing of the redox chemistry we had seen before. The concentration of the cesium salt had to reach above ∼2.0 M Cs^+ to stop the reduction of the uranium to U^{IV} [an excess of $CsNO_3$ only led to the formation of oxidized uranium(VI) phosphate]. The compound formed was **0**, which was previously made at room temperature and where we have protonated phosphite oxygen atoms in the structure. While is quite interesting, it has not yet lead to any of the other structures shown here or any other new structures thus far. However, like the formation of **1**, the mother liquors where **0** was found were still quite yellow and never precipitated any crystals when slowly evaporated. Thus far, there does not seem to be an easy way to increase the pH of the system without introducing more cations or complicating the system. Additionally, when using a normal reaction ratio (8:1:20 Cs_2CO_3−U−H_3PO_3) and simply adding acid (either HCl or H_2SO_4), we only form the reduced uranium(IV) phosphite (**1**), which seems to further the idea that the pH is the main cause for this slowing of the reduction of U^{VI} to U^{IV}.

The cations present also have a major effect on the products that form. It seems clear that the sizes of these alkali metals are either crucial to stabilizing phosphite from oxidation to phosphate or essential to forming uranium phosphite structures from oversimple uranium phosphates. There were limited problems in synthesizing the compounds listed above when using cesium, and the system is quite rich; however, there were issues with the smaller alkali salts. Results with rubidium are difficult to replicate but also yielded a very limited system with only the two structures described here dominating the reaction products. When we attempted to use the smaller potassium, sodium, and lithium, only uranyl phosphates were formed. These compounds were normally of the autunite or *meta*-autunite families. Even when we attempted to use different pH values or different salts (chloride, carbonate, etc.) or even extremely high concentrations, uranyl phosphates again were the only products formed. While there are several possible reasons for the formation of these structures, it may be that the size or relative hardness of the cation plays a role in stabilizing the phosphite ion from oxidation (thermal or otherwise) to phosphate.

CONCLUSIONS

Through the use of hydrothermal synthesis and the in situ redox reactions, we were able to elucidate the complex and fascinating chemistries within this system by simply changing the alkali carbonate concentrations and time. As one increases the cesium carbonate concentration, there is a slowing of the reduction of the U^{VI} present, which leads to the formation of more interesting, mixed-valent compounds. Additionally, as the length of the reaction time is extended, we observe the transformation of uranium(VI) phosphites to mixed-valent uranium and/or phosphorus species to the final products of uranium(IV) phosphates, with the only exception being the lowest cesium carbonate concentrations used, where the final product is only uranium(IV) phosphite.

While the products listed above help to illuminate the complexities of hydrothermal redox reactions, they also serve as a route to producing new uranium(IV) phosphates. Additionally, the U^{IV} compounds produced here have interesting environments of both six- and seven-coordinate uranium. Phosphorous acid is a unique way to convert the more soluble U^{VI} to U^{IV} and complex it with the oxidized phosphate ligand to give stable extended structures. With the exception of reactions conducted at high phosphite concentrations and very low pH, when there are even small amounts of phosphate produced in solution, the major product will normally have some phosphate in the structure, if not containing only phosphate. This may rely heavily on the solubility of the products controlling the

dx.doi.org/10.1021/ic3000735 | Inorg. Chem. 2012, 51, 6548−6558

crystalline materials observed. In general, it seems that uranium phosphates are less soluble than uranium phosphites. Furthermore, when uranium(IV) phosphite (**1**) is formed, the mother liquors are still quite dark green, and even when compound **0** is formed hydrothermally, the mother liquor is still an intense yellow color. Neither produces any more crystals when allowed to sit at room temperature or when slowly evaporated, yielding only viscous solutions. While work in these and other systems is ongoing, the products formed are greatly affected by the alkali carbonate concentration, the size of the alkali metal used, and the length of the reaction time. Thus far, it is clear that these three components, and possibly the phosphite concentrations too, collectively yield crystalline products that rely heavily on the solubility of the hydrothermally forming intermediates to generate the crystalline materials observed here.

■ ASSOCIATED CONTENT

Supporting Information

X-ray crystallographic data in CIF format, bond lengths, UV−vis−NIR absorbances, crystal pictures, powder diffraction data, and BVS calculations for all of the compounds listed. This material is available free of charge via the Internet at http://pubs.acs.org.

■ AUTHOR INFORMATION

Corresponding Author

*E-mail: e.alekseev@fz-juelich.de (E.V.A.), talbrec1@nd.edu (T.E.A.-S.). Fax: (+01)574-631-9236.

Notes

The authors declare no competing financial interest.

■ ACKNOWLEDGMENTS

We are grateful for support provided as part of the Materials Science of Actinides, an Energy Frontier Research Center, funded by the U.S. Department of Energy, Office of Science, Office of Basic Energy Sciences, under Award DE-SC0001089. We also thank the Center for Sustainable Energy at Notre Dame for use of their instrumentation.

■ REFERENCES

(1) Tabuteau, A.; Pages, M.; Livet, J.; Musikas, C. J. *Mater. Sci. Lett.* **1988**, *7*, 1315.
(2) Begg, B. D.; Vance, E. R.; Conradson, S. D. *J. Alloys Compd.* **1998**, *271*, 221.
(3) Dacheux, N.; Thomas, A. C.; Chassigneux, B.; Pichot, E.; Brandel, V.; Genet, M. *Mater. Res. Soc. Symp. Proc.* **1999**, *556*, 85.
(4) Dacheux, N.; Thomas, A. C.; Chassigneux, B.; Pichot, E.; Brandel, V.; Genet, M. *Ceram. Trans.* **1999**, *93*, 373.
(5) Kitaev, D. B.; Volkov, Y. F.; Orlova, A. I. *Radiochemistry.* **2004**, *46*, 211.
(6) Volkov, Y. F.; Tomilin, S. V.; Orlova, A. I.; Lizin, A. A.; Spiryakov, V. I.; Lukinykh, A. N. *Russ. J. Inorg. Chem.* **2005**, *50*, 1660.
(7) Wellman, D. M.; Mattigod, S. V.; Parker, K. E.; Heald, S. M.; Wang, C.; Fryxell, G. E. *Inorg. Chem.* **2006**, *45*, 2382.
(8) (a) Bray, T. H.; Nelson, A. G. D.; Jin, G. B.; Haire, R. G.; Albrecht-Schmitt, T. E. *Inorg. Chem.* **2007**, *46*, 10959. (b) Nelson, A. G. D.; Bray, T. H.; Zhan, W.; Haire, R. G.; Sayler, T. S.; Albrecht-Schmitt, T. E. *Inorg. Chem.* **2008**, *47*, 4945. (c) Nelson, A. G. D.; Bray, T. H.; Albrecht-Schmitt, T. E. *Angew. Chem., Int. Ed.* **2008**, *47*, 6252. (d) Nelson, A. G. D.; Bray, T. H.; Stanley, F. A.; Albrecht-Schmitt, T. E. *Inorg. Chem.* **2009**, *48*, 4530. (e) Diwu, J.; Nelson, A. G. D.; Albrecht-Schmitt, T. E. *Comments Inorg. Chem.* **2010**, *31*, 46. (f) Diwu, J. A.; Wang, S. A.; Liao, Z.; Burns, P. C.; Albrecht-Schmitt, T. E. *Inorg. Chem.* **2010**, *49*, 10074.
(9) (a) Koskenlinna, M.; Valkonen, J. *Acta Crystallogr.* **1996**, *C52*, 1857. (b) Cooper, M. A.; Hawthorne, F. C. *Can. Mineral.* **2001**, *39*, 797. (c) Almond, P. M.; Peper, S. M.; Bakker, E.; Albrecht-Schmitt, T. E. *J. Solid State Chem.* **2002**, *168*, 358. (d) Sullens, T. A.; Almond, P. M.; Byrd, J. A.; Beitz, J. V.; Bray, T. H.; Albrecht-Schmitt, T. E. *J. Solid State Chem.* **2006**, *179*, 1192. (e) Bray, T. H.; Skanthakumar, S.; Soderholm, L.; Sykora, R. E.; Haire, R. G.; Albrecht-Schmitt, T. E. *J. Solid State Chem.* **2008**, *181*, 493.
(10) (a) Brandstätter, F. *Z. Kristallogr.* **1981**, *155*, 193. (b) Namboodiri, P. N.; Tripathi, S. N. *J. Mater. Sci.* **2000**, *35*, 337. (c) Almond, P. M.; Albrecht-Schmitt, T. E. *Inorg. Chem.* **2002**, *41*, 5495. (d) Woodward, J. D.; Albrecht-Schmitt, T. E. *J. Solid State Chem.* **2005**, *178*, 2922. (e) Ling, J.; Ward, M.; Burns, P. C. *J. Solid State Chem.* **2011**, *184*, 401.
(11) (a) Tsivadze, A. Y.; Krot, N. N.; Muchnik, B. I. *Proc. Moscow Symp. Chem. Transuranium Elem.* **1976**, 89. (b) Bean, A. C.; Ruf, M.; Albrecht-Schmitt, T. E. *Inorg. Chem.* **2001**, *40*, 3959. (c) Sykora, R. E.; McDaniel, S. M.; Wells, D. M.; Albrecht-Schmitt, T. E. *Inorg. Chem.* **2002**, *41*, 5126. (d) Bray, T. H.; Ling, J.; Choi, E. S.; Brooks, J. S.; Beitz, J. V.; Sykora, R. E.; Haire, R. G.; Stanbury, D. M.; Albrecht-Schmitt, T. E. *Inorg. Chem.* **2007**, *46*, 3663.
(12) Chretien, A.; Kraft, J. C.; Hebd., R. *Seances Acad. Sci.* **1937**, *204*, 1936.
(13) Avduevskaya, K. A.; Rozanov, I. A.; Mironova, V. S. *Inorg. Mater.* **1977**, *13*, 1515.
(14) Avduevskaya, K. A.; Ragulina, N. B.; Rozanov, I. A. *Inorg. Mater.* **1981**, *17*, 834.
(15) Mistryukov, V. E.; Mikhailov, Y. N. *Koord. Khim.* **1985**, *11*, 1393.
(16) Doran, M.; Walker, S. M.; O'Hare, D. *Chem. Commun.* **2001**, 1988.
(17) Xu, J. F.; Li, H. H.; Cao, Y. N.; Huang, C. C.; Zhang, H. H.; Lin, D. S.; Yang, Q. Y.; Sun, R. Q. *Chinese J. Struct. Chem.* **2006**, *25*, 1380.
(18) Mandal, S.; Chandra, M.; Natarajan, S. *Inorg. Chem.* **2007**, *46*, 7935.
(19) Villa, E. M.; Wang, S.; Alekseev, E. V.; Depmeier, W.; Albrecht-Schmitt, T. E. *Eur. J. Inorg. Chem.* **2011**, 37494.
(20) (a) Burns, P. C.; Miller, M. L.; Ewing, R. C. *Can. Mineral.* **1996**, *34*, 845. (b) Burns, P. C.; Ewing, R. C.; Hawthorne, F. C. *Can. Mineral.* **1997**, *35*, 1551. (c) Burns, P. C. In *Uranium: Mineralogy, Geochemistry and the Environment*; Burns, P. C., Finch, R., Eds.; Mineralogical Society of America: Washington, DC, 1999; Chapter 1. (d) Burns, P. C. *Mater. Res. Soc. Symp. Proc.* **2004**, *802*, 89. (e) Burns, P. C. *Can. Mineral.* **2005**, *43*, 1839. (f) Burns, P. C. In *Structural Chemistry of Inorganic Actinide Compounds*; Krivovichev, S. V., Burns, P. C., Tananaev, I. G., Eds.; Elsevier:: Amsterdam, The Netherlands, 2007; Chapter 1.
(21) (a) Kepert, D. L.; Patrick, J. M.; White, A. H. *J. Chem. Soc., Dalton Trans.* **1983**, 381. (b) Bombieri, G.; Benetollo, F.; Klahne, E.; Fischer, D. *J. Chem. Soc., Dalton Trans.* **1983**, 1115. (c) Benard, P.; Louer, D.; Dacheux, N.; Brandel, V.; Genet., M. *Chem. Mater.* **1994**, *6*, 1049. (d) Allen, S.; Barlow, S.; Halasyamani, P.; Mosselmans, J.; O'Hare, D.; Walker, S. M.; Walton, R. I. *Inorg. Chem.* **2000**, *39*, 3791. (e) Wang, C. M.; Liao, C. H.; Lin, H. M.; Lii, K. H. *Inorg. Chem.* **2004**, *43*, 8239. (f) Berthet, J. C.; Thuery, P.; Dognon, J. P.; Guillaneux, D.; Ephritikhine, M. *Inorg. Chem.* **2008**, *47*, 6850. (g) Lin, C. H.; Lii, K. H. *Angew. Chem.* **2008**, *120*, 8839. (h) Mougel, V.; Horeglad, P.; Nocton, G.; Pecaut, J.; Mazzanti, M. *Angew. Chem., Int. Ed.* **2009**, *48*, 8477. (i) Andreev, G.; Budantseva, N.; Tananaev, I.; Myasoedov, B. *Inorg. Chem. Commun.* **2010**, *13*, 577. (j) Nguyen, Q. B.; Liu, H. K.; Chang, W. J.; Lii, K. H. *Inorg. Chem.* **2010**, *50*, 4241.
(22) (a) Burns, P. C.; Finch, R. J.; Hawthorne, F. C.; Miller, M. L.; Ewing, R. C. *J. Nucl. Mater.* **1997**, *249*, 199. (b) Burns, P. C.; Finch, R. J. *Am. Mineral.* **1999**, *84*, 1456. (c) Belai, N.; Frisch, M.; Liton, E.; Ravel, B.; Cahill, C. L. *Inorg. Chem.* **2008**, *47*, 10135.

(23) *SADABS, Program for absorption correction using SMART CCD based on the method of Blessing*: Sheldrick, G. M.; Blessing, R. H. *Acta Crystallogr.* **1995**, *A51*, 33.
(24) (a) Halasyamani, P. S.; Francis, R. J.; Walker, S. M.; O'Hare, D. *Inorg. Chem.* **1999**, *38*, 271. (b) Krivovichev, S. V.; Burns, P. C. *J. Solid State Chem.* **2002**, *168*, 245. (c) Krivovichev, S. V.; Burns, P. C. *Can. Mineral.* **2003**, *41*, 707. (d) Krivovichev, S. V.; Burns, P. C. *Can. Mineral.* **2005**, *43*, 713. (e) Rastsvetaeva, R. K.; Barinova, A. V.; Fedoseev, A. M.; Budantseva, N. A.; Nekrasov, Yu. V. *Dokl. Akad. Nauk* **1999**, *365*, 68. (f) Andreev, G. B.; Antipin, M. Yu.; Fedoseev, A. M.; Budantseva, N. A. *Koord. Khim.* **2001**, *27*, 227. (g) Khrustalev, V. N.; Andreev, G. B.; Antipin, M. Yu.; Fedoseev, A. M.; Budantseva, N. A.; Shirokova, I. B. *Zh. Neorg. Khim.* **2000**, *45*, 1996. (h) Krivovichev, S. V.; Locock, A. J.; Burns, P. C. *Z. Kristallogr.* **2005**, *220*, 10. (i) Krivovichev, S. V.; Finch, R. J.; Burns, P. C. *Can. Mineral.* **2002**, *40*, 193. (j) Krivovichev, S. V.; Tananaev, I. G.; Kahlenberg, V.; Myasoedov, B. F. *Dokl. Phys. Chem.* **2005**, *403*, 124. (k) Mikhailov, Yu. N.; Gorbunova, Yu. E.; Baeva, E. E.; Serezhkina, L. B.; Serezhkin, V. N. *Zh. Neorg. Khim.* **2001**, *46*, 2017.
(25) Krivovichev, S. V.; Burns, P. C. In *Structural Chemistry of Inorganic Actinide Compounds*; Krivovichev, S. V., Burns, P. C., Tananaev, I. G., Eds.; Elsevier:: Amsterdam, The Netherlands, 2007; Chapter 4.
(26) (a) Krivovichev, S. V.; Gurzhii, V. V.; Tananaev, I. G.; Myasoedov, B. F. *Dokl. Phys. Chem.* **2006**, *409*, 228. (b) Budantseva, N. A.; Andreev, G. B.; Fedoseev, A. M.; Antipin, M. Yu. *Russ. J. Coord. Chem.* **2003**, *29*, 653. (c) Grigor'ev, M. S.; Fedoseev, A. M.; Budantseva, A. A.; Bessonov, A. A.; Krupa, J.-C. *Crystallogr. Rep.* **2004**, *49*, 676.

dx.doi.org/10.1021/ic3000735 | *Inorg. Chem.* 2012, 51, 6548−6558